Interaction of Monodisperse Anionic Amphiphiles with the i-Face of Secreted Phospholipase A_2[†]

Bao-Zhu Yu,[‡] Rafael Apitz-Castro,[‡] Ming-Daw Tsai,[§] and Mahendra K. Jain*[,‡]

Department of Chemistry and Biochemistry, University of Delaware, Newark, Delaware 19716, and Department of Chemistry and Biochemistry, The Ohio State University, Columbus, Ohio 43210

Received February 10, 2003; Revised Manuscript Received April 1, 2003

ABSTRACT: Pancreatic IB phospholipase A_2 (PLA2) forms aggregates of defined size with monodisperse alkyl sulfates in the premicellar concentration range. As an extension of the interfacial kinetic paradigm, results are interpreted in terms of a model in which several amphiphile molecules bind along their polar headgroup to the interface binding region (i-face) of PLA2. The resulting complex, $E^{\#}$, has a half-micellar structure, and it acts as an "amphiphile" in the aqueous phase. $E^{\#}$ not only self-aggregates but also binds hydrophobic probes and interacts with hydrophobic surfaces. As expected, resonance energy transfer from the tryptophan donor in PLA2 to an acceptor probe partitioned in $E^{\#}$ shows a biphasic dependence as the probe coexisting with PLA2 is diluted at higher alkyl sulfate concentrations. The gel-permeation behavior of PLA2 at premicellar alkyl sulfate concentrations is also biphasic. For example, above 1.2 mM decyl sulfate (CMC = 3.5 mM) PLA2 elutes as a single sharp peak, presumably the self-aggregate of $E^{\#}$ with apparent molecular mass of 120−150 kDa. At 0.4−1 mM decyl sulfate the retention volume is even larger than that for the 14 kDa PLA2. This anomalous retention is attributed to the interaction of the hydrophobic region of $E^{\#}$ with the hydrophobic patches on the gel-permeation matrix. Elution behavior of the self-aggregated $E^{\#}$ form of site-directed mutants in dodecyl sulfate suggests that certain substitutions in the conserved hydrogen-bonding network have a significant effect on the aggregate size. These results suggest a role for the network in the amphiphile binding along the i-face of PLA2, presumably through a change in the anion coordination ligands.

Interfacial enzymes access their substrate for processive catalytic turnover by binding to the substrate interface (*1*−*5*). The paradigm of the interface binding region (the i-face)[1] distinct from the catalytic site has guided quantitative resolution of the events of the interfacial turnover cycle (*6*, *7*) and the allosteric K_S* (*8*) and k_{cat}* activation (*9*−*11*) of secreted phospholipase A_2 (PLA2). Binding of PLA2 along the i-face involves scores of amphiphiles in the interface (*12*). The quantitative focus of the interfacial kinetic paradigm is based on the tight binding of PLA2 to the preformed interfaces where the substrate does not exchange between the coexisting interfaces or it exchanges rapidly on the time scale of the turnover time (*5*). This is because equilibrium and dynamics of the interface binding step have diverse consequences. Also such interactions influence the interface preference and allosteric regulation (*4*, *5*) of the PLA2 orthologues (*13*). For example, the human group X PLA2 shows nearly equal preference for the zwitterionic and anionic substrates (*14*, *15*). On the other hand, IB and IIA PLA2 show a preference for the anionic but not the zwitterionic interface (*16*, *17*). Also, complex kinetic and binding behaviors of PLA2 with substrates and amphiphile additives have been attributed to the "quality of interface" (*18*−*29*) that controls the enzyme and substrate exchange between the interfaces (*5*). Also, the origin of other anomalous kinetic effects has been shown to be in kinetic paths on extraneous surfaces present in the reaction mixture, such as the vessel walls and air bubbles (*30*, *31*).

A general description of the amphiphile binding along the i-face of PLA2, and of its coupling to the events at the active site, remains to be established. As an elaboration to the interfacial kinetic paradigm, we propose a heuristic model (Figure 1) to guide understanding of the amphiphile binding to the i-face of PLA2. Operationally, the binding of E to a preformed interface (A*) to form E* is treated as a single step. This acknowledges the fact that interaction of scores of amphiphiles with dozens of residues on the i-face of the enzyme cannot be meaningfully dissected (*1*, *4*−*6*, *12*, *32*). As conceptualized in the lower half of Figure 1, as a first step toward understanding the amphiphile interactions along the i-face, we propose that PLA2 interacts with several monodisperse amphiphiles to form $E^{\#}$. It is a half-micellar complex. The thermodynamics of such amphiphile−enzyme interactions along the i-face is different from that of the amphiphile−amphiphile interactions that stabilize the amphiphile aggregate A*. Preferential interaction of the head-

[†] The research was supported by NIH Grants GM-29703 (M.K.J.) and GM-41788 (M.-D.T.).

* To whom correspondence should be addressed. Telephone: 302-831-2968. Fax: 302-831-6335. E-mail: mkjain@udel.edu.

[‡] University of Delaware.

[§] The Ohio State University.

[1] Abbreviations: CMC, critical micellization concentration; EDTA, ethylenediaminetetraacetic acid; EGTA, ethylene glycol bis(β-aminoethyl ether)-*N*,*N*,*N*′,*N*′-tetraacetic acid; HDNS, *N*-dansylhexadecylphosphoethanolamine; i-face, the interface binding surface of an interfacial enzyme; PLA2, secreted 14 kDa type IB phospholipase A_2 from pig or bovine pancreas; RET, resonance energy transfer.

10.1021/bi034232x CCC: $25.00 © 2003 American Chemical Society
Published on Web 04/30/2003

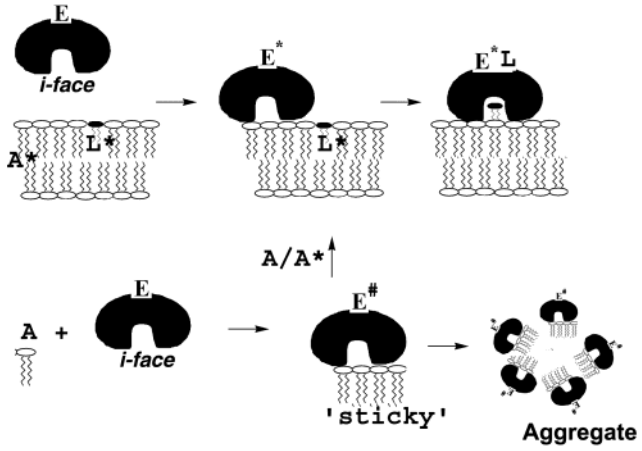

FIGURE 1: A heuristic model for the binding of an interfacial enzyme (E) with an amphiphile. (Upper) E* is formed when free enzyme E binds preferentially along the i-face, the interface binding region, to a preformed interface (A*) of an amphiphile such as micelle or vesicle. E, A*, and E* are thermodynamically stable. E is catalytically inert and E* is catalytically active. L* is the active site-directed molecule partitioned in the interface. (Lower) The key concept developed in this paper is that $E^{\#}$ is formed as the headgroup of A interacts with the i-face. With several exposed acyl chains $E^{\#}$ would behave like an amphiphile that can stick to hydrophobic surfaces or self-aggregate. In effect, the solution behavior of $E^{\#}$ is expected to be quite different from that of E, A, E*, and A*.

groups of monodisperse A with PLA2 to form $E^{\#}$ would be at concentrations well below the CMC, whereas A* is formed above the CMC. $E^{\#}$ is an "amphiphile" because the hydrophobic drive of the exposed acyl chains has consequences for its stability and the solution behavior. In comparison, such forces are in thermodynamic equilibrium in the E, E*, or A* micelle or bilayer vesicle.

Results in this paper show that IB PLA2 forms large aggregates in the presence of monodisperse alkyl sulfates. Aggregation is interpreted as a consequence of the formation of $E^{\#}$ which self-aggregates, "sticks" to hydrophobic surfaces, and partitions hydrophobic probes. The key result is that $E^{\#}$ is formed in the absence of the catalytic cofactor calcium or an active site-directed ligand. It is intriguing that the size of the aggregate of $E^{\#}$ remains virtually constant over a wide range of amphiphile concentration. Surprisingly, however, certain site-directed mutants, particularly those with changes in the hydrogen bond network, form aggregates of different size. Starting with the suggestion that the change in the aggregation behavior of $E^{\#}$ amphiphile is related to its shape, results are interpreted to suggest that the residues of the hydrogen-bonding network introduce significant structural changes in the ligands for the anionic headgroup interactions for the binding of the amphiphiles along the i-face of PLA2.

EXPERIMENTAL PROCEDURES

Alkyl sulfates were from Aldrich or Acros. Sources for other reagents (*6*−*11*, *33*−*35*) and enzymes and mutants (*32*, *36*) were described before. All measurements were carried out at pH 6.9 and 24 °C in the standard buffer containing 0.48 M NaCl, 20 mM Tris, 10 mM HEPES, and other additives as noted.

Critical Micellization Concentration (CMC). Surface tension was monitored with a Wilhelmy balance (*7*). The CMC value was determined from the plot of the change in the surface tension of the standard buffer as a function of the amphiphile concentration on the logarithmic scale. The change in the surface tension is defined as the surface pressure. By definition the surface tension of the aqueous phase reaches its minimum at the CMC. The CMC values of the three homologous alkyl sulfates used in this study are summarized in Table 1. These values are consistent with those determined in the presence of suitable spectroscopic probes. Controls with decyl sulfate showed that its CMC value did not change significantly in the presence of 0.5 mM calcium and also in the presence of 20 μM PLA2. It implies that the $E^{\#}$ complex does not partition preferentially into the air−water interface. Also note that even if a dozen amphiphile molecules bind to each PLA2 molecule and the complex remained in the aqueous phase, under these conditions the change in the effective amphiphile concentration at the CMC would be about 0.2 mM.

Table 1: Aggregate Size[a] for Pig PLA2 in the Presence of Alkyl Sulfate

amphiphile	CMC (mM)	MW (kDa)
octyl sulfate	35	50 (at 25 mM)
decyl sulfate	3.5	120 (at 1.2 mM)
dodecyl sulfate	0.25	150 (at 0.2 mM)

[a] These measurements were made in the standard elution buffer containing the indicated amphiphile concentration. Uncertainty in the apparent molecular mass (MW) is 20%.

Apparent Molecular Mass by Size-Exclusion Chromatography. The retention volume for PLA2 was obtained with gel-permeation columns preequilibrated and eluted with the standard buffer in the presence of suitable additives and amphiphiles at the indicated concentrations. Typically, 4−8 μg of protein was injected through a 5 or 20 μL loop. During elution the flow rate was kept constant at 1.0 mL/min for the next 25−50 min. Elution of PLA2 was monitored on the Rainin HPLC system with duel pump and sequentially equipped with the UV absorbance and fluorescence detectors. Simultaneous monitoring of the absorbance (280 nm) and fluorescence (excitation at 280 nm, emission at 340 nm) eliminated most artifacts for a qualitative analysis of the elution profile. The detector (15 μL volume for the flow cells) output included significant scattering contributions, which precludes quantitative analysis of the peak intensities to estimate the eluted protein.

The elution buffer and flow rate are optimum for several calibration standards. Such an ideal behavior is expected if the protein does not interact with the column matrix. Results reported in this paper were obtained on two different columns: an 8 × 300 mm glass column, Protein-Pak 300 SW from Waters, or a 7.5 × 250 mm Bio-Sil SEC-250 from Bio-Rad. The calibration curve shown in Figure 2, or its equivalent for the other column, was used for the calculation of the apparent molecular mass. On both of the columns the apparent molecular masses of several secreted PLA2 (MW 14−15 kDa) were between 12 and 13 kDa. Possible aggregation of PLA2 in the aqueous phase is therefore ruled out, although as noted later a modest interaction of PLA2 with the gel-permeation matrix is likely. The matrix from both the columns is chemically similar, yet the size-exclusion behavior, resolution, stability, and batch-to-batch variability was found to be significantly different. The long-term stability of the Protein-Pak column operated at lower pressures is noticeably better.

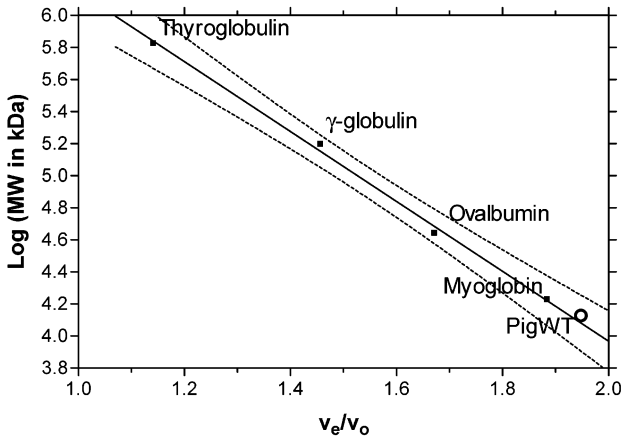

FIGURE 2: Plot of log(MW) versus relative elution volume (v_e/v_0) from a Bio-Sil SEC-250 column for the calibration standards in the standard buffer (0.475 M NaCl, 1 mM EGTA, 1 mM EDTA, and 20 mM Tris at pH 7.5). The pig pancreatic PLA2 (14.3 kDa) is retained marginally longer with an apparent MW of 13.5 kDa. The retention volume of blue dextran or protein aggregate was taken as v_0 (5.00 min), the void volume. Only a truncated calibration curve is shown; however, it is linear up to the calibration standard of 1.2 kDa. The dotted lines show the 95% confidence limit for the linear fit (continuous line).

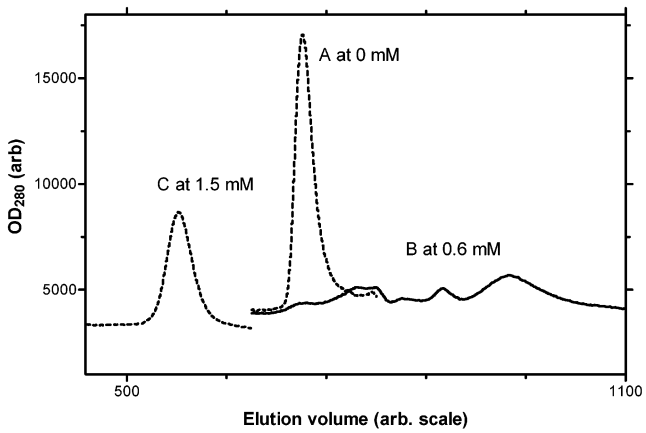

FIGURE 3: Elution profiles for PLA2 in (A) standard buffer containing 1 mM EGTA and 1 mM EDTA alone and with (B) 0.6 mM or (C) 1.5 mM decyl sulfate. Only the region of the protein elution is shown. The abscissa and ordinate scales (arbitrary) are the same for the three runs.

Emission from the Resonance Energy Transfer. Steady-state florescence measurements in the standard buffer in a quartz cuvette under the specified conditions were carried out on an SLM-Aminco AB2 instrument set in the ratio mode with slit widths of 4 nm for the emission and excitation wavelengths. The intensity of the RET signal from the HDNS acceptor was monitored at 500 nm with excitation at 280 nm for the only tryptophan residue (W3) in PLA2. Typically, for these measurements the order of addition was buffer, 1 μM HDNS, and 1 μM PLA2, followed by successive addition of a concentrated solution of the amphiphile. The signal intensities were corrected for the dilution.

RESULTS

The main goal of this study is to characterize the complex formed by the interaction of homologous monodisperse alkyl sulfate with PLA2. As conceptualized in Figure 1, the $E^{\#}$ complex is an amphiphile with a half-micellar structure which is likely to be thermodynamically unstable in the aqueous phase. The hydrophobicity and effective shape of $E^{\#}$, and therefore the properties of its aggregates, will depend on the number of the bound amphiphiles and also the length of the exposed acyl chains. Results in this section show that the $E^{\#}$ form of PLA2 self-aggregates, interacts with hydrophobic surfaces, and partitions probes. The aggregate size depends not only on the chain length of alkyl sulfate but also on the subtle changes in the structure of PLA2 introduced at certain residues by site-directed mutagenesis.

Effect of Decyl Sulfate on Gel-Permeation Behavior of PLA2. The salt concentration and pH in the elution buffer is optimized to eliminate the ionic interactions of the gel-permeation matrix with the calibration standards. The elution volume of pig PLA2 from gel-permeation columns is typically 5−10% more than that predicted from the calibration standards. Anomalous retention is expected if the eluting species interacts with the matrix. As shown in Figure 3, the elution volume for pig PLA2 shows a complex dependence on the decyl sulfate concentration in the elution buffer: As shown by profile A, from 0 to 0.4 mM decyl sulfate the protein elutes as a single peak of about 14 kDa. As shown by profile B, between 0.5 and 1.2 mM decyl sulfate the protein elutes in several broad peaks of larger retention volume. Multiple peaks are observed at the intermediate concentrations. We attribute the anomalous retention to specific interaction of the column matrix with $E^{\#}$. Such interactions are analogous to those that dominate the adsorption chromatographic behavior on a reverse-phase matrix. If so, multiple peaks could come from multiple affinity sites on the matrix. At this stage we cannot rule out other explanations based on the formation of multiple PLA2-containing species. For example, one of the effects of increasing the amphiphile concentration would be to saturate the hydrophobic patches on the column matrix. This will promote self-aggregation of $E^{\#}$ as the patches become less hydrophobic. This interpretation is consistent with the fact that at higher amphiphile concentrations all of the protein elutes in a single sharp peak with virtually the same calculated aggregate size on several different makes of the gel-permeation columns.

The position of peak C in Figure 3 corresponds to an apparent molecular mass of 120−150 kDa. It is based on the assumption that the gel-permeation behavior of the aggregate is analogous to that for the globular proteins used as the calibration standards, that in effect the aggregate is "globular" and that it does not have anomalous interaction with the gel-permeation matrix. Compared to the typical aggregation number of 50−70 kDa for the alkyl sulfate micelles, the 120−150 kDa aggregate may contain several PLA2 molecules. At this stage we do not have a method to determine the enzyme-to-amphiphile ratio in the aggregate.

Amphiphile concentration dependence of the transition from anomalous retention to the elution of the aggregate is instructive. As summarized in Figure 4, the faster eluting sharp peak C begins to appear at 0.8 mM decyl sulfate. Beyond 1.2 mM decyl sulfate virtually all of the protein elutes in this peak. These results show that the 120 kDa aggregate is formed well below the CMC of decyl sulfate (3.5 mM). On the basis of the sharp increase in the area of this peak, aggregate formation could be a cooperative process. Also note that the aggregate formation occurs at 20

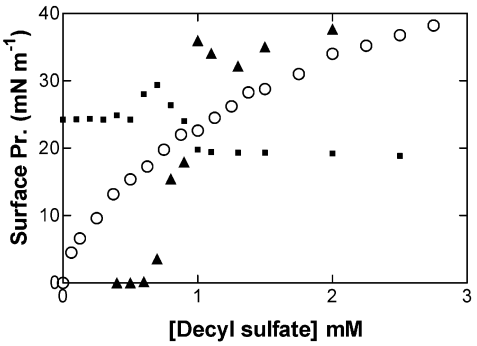

FIGURE 4: Effect of decyl sulfate concentration (CMC = 3.5 mM) on the (unfilled circles) surface pressure defined as the decrease in the surface tension of the air/buffer surface. The area of the fastest eluting aggregate (peak C in Figure 3) increases sharply. Note that the changes in the elution behavior of PLA2 (given on arbitrary scales) occur in the range of 15−30 mN/m surface pressure. The onset of micellization occurs at 35 mN/m or 3.4 mM decyl sulfate (given as the CMC values in Table 1). All measurements were in the standard buffer containing 1 mM EGTA and 1 mM EDTA.

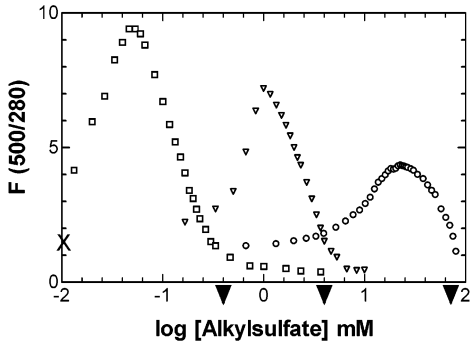

FIGURE 5: Change in the RET signal intensity at 500 nm on the titration of a mixture of 1 μM pig PLA2 and 1 μM monodisperse HDNS (CMC = 12 μM) in the standard buffer containing 1 mM EGTA and 1 mM EDTA with (from left) dodecyl sulfate (squares), decyl sulfate (triangles), or octyl sulfate (circles) concentration (on the logarithmic scale). The dark arrows (along the *x*-axis) mark the CMC (Table 1) for the three homologous amphiphiles. The signal on the addition of PLA2 to HDNS (without any alkyl sulfate in the buffer) is marked with a × on the ordinate.

mN/m surface pressure. It is well below the saturating pressure for the onset of micellization at 40 mN/m. Put another way, the surface pressure of the decyl sulfate in E$^{\#}$ is about half of the surface pressure in its micelles.

Anomalous retention of PLA2 at intermediate decyl sulfate concentrations depends on the state of the gel-permeation matrix. Also, the anomalous behavior is independent of the size-exclusion characteristics of the matrix. Different makes of the column or different batches from the same supplier show significant differences in the slope of the calibration curve and also the anomalous retention characteristics of PLA2 in the presence of monodisperse alkyl sulfates. With a new column the calibration curve is reproducible to within 3% with an estimated uncertainty of 10% in the apparent molecular mass. During the slow deterioration of the gel-permeation matrix over a period of time, the anomalous retention was noticeable much earlier than a change in the gel-permeation behavior for the larger aggregates or the protein standards. Typically, with a new column the anomalous retention volumes were reproducible for the first 80−100 runs. In comparison, calibration with the noninteracting standards remained acceptable for another several hundred runs. According to the suppliers, density and distribution of the hydrophobic patches cannot be adequately characterized. Complex interactions with the gel-permeation matrix make it difficult to characterize the E$^{\#}$ complex by this method. For such reasons we made little further attempt to characterize the significance of the anomalous retention volumes.

The Aggregate Size Changes with the Chain Length. It is intriguing that the size of the aggregate formed above the CMC of decyl sulfate is the same as that of the aggregate formed below the CMC (results not shown). However, as summarized in Table 1, the apparent molecular mass of the aggregate formed at the premicellar concentrations of the three homologous alkyl sulfates increases with the chain length. According to the model in Figure 1, if the retention volume is related only to the size-exclusion behavior, as discussed later the aggregate size would depend on the effective shape of E$^{\#}$ for packing in the aggregate.

Resonance Energy Transfer (RET) from PLA2 to HDNS in the Presence of Monodisperse Alkyl Sulfate. A fluorescence protocol, which circumvents problems associated with the extraneous surfaces (*31*), takes advantage of the fact that a hydrophobic probe, HDNS, partitions fully into E$^{\#}$ or its aggregate. As the acceptor and donor pair for RET, HDNS−PLA2 provides information about the microenvironment in which they are colocalized (*32*, *33*). As shown in Figure 5, the RET signal intensity shows a biphasic dependence on the concentration of alkyl sulfate added to 1 μM PLA2 and 1 μM HDNS (CMC = 10 μM). The signal increases initially as the tryptophan donor in PLA2 and the dansyl acceptor in HDNS are colocalized in the same complex. The intensity decreases at the higher concentrations as HDNS in the complex is competitively replaced by alkyl sulfate. With excess alkyl sulfate, the residual signal is virtually the same as with a mixture of HDNS and micellar alkyl sulfate without PLA2 (not shown). Not only the increase but also a large part of the decrease in the RET signal occurs below the CMC of the amphiphile. For the three homologous alkyl sulfates in Figure 5 the RET intensity at the CMC is less than 20% of the peak intensity. The biphasic change in the RET signal was not obtained with W3F PLA2. The biphasic concentration dependence is also seen in the tryptophan emission; however, as expected the signal decreases initially and then it increases. These and other controls show that the signal in Figure 5 is due the energy transfer from Trp-3 of PLA2 to HDNS colocalized in the same aggregate.

The RET peak intensity increases with the amphiphile chain length (Figure 5). In terms of the model in Figure 1 the effect could come from enhanced energy transfer or lesser quenching by water of HDNS in the E$^{\#}$ complex with the longer chain amphiphile. Explanations based on the preferential binding of HDNS to the active site of PLA2 can be ruled out because these measurements were made in the absence of calcium, which is a cofactor for the binding of active site-directed ligands to PLA2 (*35*). It is likely that the site for the initial binding of HDNS may be one of the amphiphile binding sites along the i-face. The signal intensity (marked as a × on the ordinate in Figure 5) from a mixture of PLA2 and monodisperse HDNS is about 15% of the peak intensity obtained with dodecyl sulfate. This initial signal is attributed to a weak affinity of HDNS for PLA2 or to a weak signal from such a complex.

Table 2: Relative Elution Volume (v_e/v_0) for IB PLA2 Mutants in 0.2 mM Dodecyl Sulfate[a]

mutant	peak I	peak II	peak III	peak IV	mutant	peak I	peak II	peak III	peak IV
					Pig WT				
WT	1.40				67W	1.40			
(Δ62−66) mutant	1.40				69K	1.40			
31R,53M	1.38				69F	1.40			
31R,56M	1.38				69F,53M	1.40			
31R,53,56M	1.38				69F,56M	1.40			
31R,69F	1.40				69F,53,56M	1.42			
52F	1.40				73F	1.42			
52L	1.40	1.84			73L	1.40	1.67		
52F,73F	1.40								
					Semisynthetic Mutants of Pig AMPA				
AMPA	1.38				4-Nle	1.38			
1-D-Ala-	1.38				Δ-1-	1.38			
1-Gly-	1.38				Δ1,2-	1.38			
W3F	1.36				Δ1−6-			2.1	
W3G		1.89			Δ1−8-		1.80		
W3Y	1.38		2.1		3-Phe-7-Ala	1.38			
					Bovine PLA2 Mutants				
WT	1.40				Y52K	1.40			
L2A	1.40				F52V	1.40			
L2R	1.40				Y52,73F	1.40			
L2W	1.40				Y52,73F, D99N		1.71		
W3A			2.0		D99N	1.42			
Q4A	1.40				D99A		1.71		
Q4E	1.40				N71E	1.42	1.71		
F5A	1.40	1.71			Y73A	1.40	1.71		
F5V	1.44	1.71			Y73F	1.40			
F5W	1.42				Y73K		1.71		
F5Y	1.40				Y73S		1.61, 1.71		
N6A	1.40				A102I	1.44			
I9A	1.40	1.71			A102S	1.44			
I9F		1.71			A103S	1.40			
I9S	1.44	1.71			F106Y	1.42			
I9Y	1.40	1.71			C27−123A	1.42			
F22A	1.42	1.69			Δ115−123		1.71		
F22I	1.44	1.61			115−122A	1.44			
F22Y	1.42	1.61			K56E	1.40			
H48A	1.40				K53M	1.40			
H48N	1.40				K53M	1.40			
H48Q	1.40				K53,56M	1.42			
D49A	1.40				K120,121A	1.40			
D49E	1.40				K53,56,120M	1.42			
D49K	1.40				K53,56,121M	1.40			
D49N	1.40				K53,120,121M	1.40			
D49Q	1.40				K56,120,121M	1.40			
Y52F	1.40				K53,56,120,121M	1.40	1.67	1.97	2.15

[a] With the calibration curve in Figure 2: v_e/v_0 of 1.94 = 14.3 kDa and of 1.37 = 150 kDa.

Together, RET results provide independent support for the formation of the $E^{\#}$ complex in which HDNS is partitioned. Qualitatively interpreted in terms of the model in Figure 1, the initial increase in the RET signal with added monodisperse alkyl sulfate is attributed to the formation of more $E^{\#}$ complexes in which HDNS is partitioned. Beyond the peak, the donor−acceptor pair is separated from each other as the alkyl sulfate competes with HDNS for a constant number of the amphiphile binding sites on the i-face. As expected, at "infinite dilution" with excess alkyl sulfate the signal intensity is virtually the same with or without PLA2. Although intuitively appealing, the number of possible primary events in this system makes it nearly impossible to arrive at a meaningful quantitative model for the RET results in Figure 5.

Aggregates of IB PLA2 Mutants with Premicellar Concentration of Dodecyl Sulfate. The gel-permeation protocol was adopted to screen the formation of $E^{\#}$ aggregates of a large number of the site-directed mutants of bovine and pig PLA2. The relative elution volume, v_e/v_0, in 0.2 mM dodecyl sulfate (CMC = 0.5 mM) for one or more peaks obtained for these mutants is summarized in Table 2. These mutants have been fully characterized and analyzed in terms of the interfacial kinetic parameters to identify the origins of their functional perturbation (*4*, *5*, *10*, *11*, *32*, *36*, *39*−*43*). According to the calibration curve a value of $v_e/v_0 = 1.94$ corresponds to 14 kDa for the E form, and $v_e/v_0 = 1.37$ corresponds to the 150 kDa aggregate formed with the aggregate of the $E^{\#}$ form with most of the mutants. None of the mutants formed larger aggregates with v_e/v_0 significantly below 1.4. To identify the perturbed binding of anionic dodecyl sulfate, the mutants of interest are those with $v_e/v_0 > 1.4$.

The rationale for the choice of the experimental conditions under which the v_e/v_0 values were obtained follows from Figure 6. The elution volume for the native (WT) PLA2

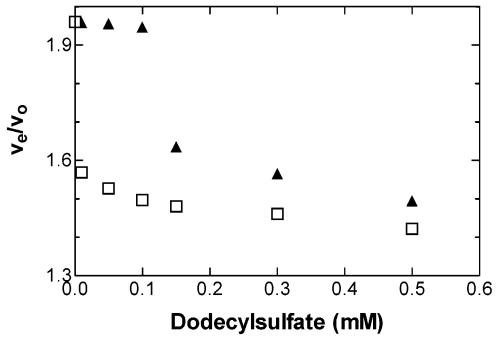

FIGURE 6: Effect of the dodecyl sulfate concentration in the elution buffer on v_e/v_0 for the fastest eluting peak of (squares) bovine PLA2 or (triangles) its K53,56,120,121M mutant from the gel-permeation column equilibrated with the amphiphile. The vertical arrows show the range of elution for the slower peaks (similar to those in peak B in Figure 3) for the quadruple mutant. Other conditions are given in Experimental Procedures and the legend to Figure 2.

changes rapidly as a function of the dodecyl sulfate concentration, and at 0.2 mM virtually all of the protein elutes as the aggregate. On the other hand, as also shown in Figure 6, the elution volume for the fastest eluting peak of the K53,56,120,121M quadruple mutant decreases at somewhat higher dodecyl sulfate concentrations. Thus in 0.2 mM dodecyl sulfate mutants with amphiphile binding comparable to WT PLA2 would elute as a single peak at $v_e/v_0 = 1.4$, whereas the mutants with perturbed amphiphile binding would show multiple peaks and larger elution volumes (Figures 3 and 6). In contrast, in 0.5 mM dodecyl sulfate the mutants with as perturbed amphiphile binding as the quadruple mutant would elute at a relative volume of 1.4. In short, on the basis of the results in Figure 6, the window of the dodecyl sulfate concentration in the elution buffer is defined by the difference between the elution behaviors of WT and the quadruple mutant. In other words, 0.2 mM dodecyl sulfate in elution buffer for the results in Table 2 is well suited to identify the mutants with the amphiphile binding weaker than that for WT. Independent controls also showed that PLA2 is not denatured at these dodecyl sulfate concentrations.

In conjunction with the results for the quadruple mutant (above) it is noteworthy that substitution of as many as three lysines has no significant effect on the elution volume (Table 2). Analysis of the kinetic results showed that K53 and K56 are not directly involved in the binding of the anionic amphiphiles at the interface, although the charge compensation of K53 and K56 is responsible for the allosteric k_{cat}* activation (*10*, *11*). The substitution of K120 and 121 influenced the binding of the enzyme to the interface as well as the binding of the substrate to the active site. These results are in general agreement with the crystal structure of the anion-assisted homodimer of PLA2 (*37*) and proPLA2 (*38*) that showed that K53 and K56 are not involved in the anion binding. Only the side chain of K121 is liganded to an anion. In fact, most of the PLA2 ligands that coordinate to the anions are not cationic but NH of the backbone amide. Therefore, it is not surprising that substitution of one, two, or three of the lysines with methionine does not interfere with the aggregation induced by the anionic amphiphile. Together, results with the lysine substitution mutants support the earlier conclusion that the binding of PLA2 to the anionic amphiphiles, monodisperse or at the interface, is dominated by close-range specific interactions with polarizable ligands such as the backbone NH and the immobilized water molecules.

Results in Table 2 are also in general accord with the paradigm that the catalytic site is distinct from the i-face. For example, the aggregate size of the k_{cat}*-impaired mutants remains virtually constant with v_e/v_0 in the 1.37−1.45 range. For example, the substitutions in the catalytic site (H48), substrate pocket (L2, Y52, F106), and the calcium-binding ligand (D49) or loop (L31) did not have a significant effect on v_e/v_0. Also the deletion of the 62−66 loop or the substitution of Y69 have little effect on v_e/v_0.

Mutants with $v_e/v_0 > 1.45$ (Table 2) form smaller aggregates, presumably due to perturbed amphiphile binding. For example, several single substitutions (W3, F5, I9, F22, N71, Y73) lower v_e/v_0 to 1.7−1.9. These residues are expected to be on the i-face. A similar change is induced by other single (D99A and N71E) and triple (Y52,73F,D99N) substitutions, as well as by the major deletions (Δ1−6, Δ1−8, and Δ115−123). On the other hand, deletion of A1 (Δ1) or A1-L2 (Δ1,2) at the N-terminus does not significantly influence the aggregation. As discussed below, these results implicate an unexpected role for the well-conserved hydrogen-bonding network in the aggregate formation, presumably through the binding of multiple anionic amphiphiles to the i-face of PLA2.

DISCUSSION

Operationally, the i-face residues of PLA2 involved in its binding to the interface are distinct from the catalytic active site residues (*1*, *4*, *5*, *12*). This paradigm has paved the way for quantitative interfacial kinetic analysis in terms of microscopic constants for the events of well-defined interfacial turnover cycle (*3*−*7*, *31*, *32*) and to resolve the factors governing allosteric activation by the interface and the interfacial anionic charge (*8*−*11*). Binding of alkyl sulfate to the i-face relates to yet another aspect of the PLA2 function that is relevant in the physiological environment of type IB and IIA PLA2: Both show a marked preference for an anionic interface (*3*−*6*, *12*, *17*). Also, anionic bile salts of the digestive tract are the natural activators of the pancreatic IB PLA2 (*39*).

Packing Constraints for Aggregation. Self-aggregation of half-micellar $E^{\#}$ follows from its amphiphilic character. The hydrophobic drive for the aggregation comes from the exposed acyl chains in $E^{\#}$. Alkyl sulfates are bound along their headgroup to the i-face of PLA2. Thus spatially separated polar and nonpolar regions in $E^{\#}$ make it an effective amphiphile for self-aggregation. Put another way, interaction of anionic amphiphiles along the i-face changes the hydrophilic to hydrophobic balance (amphiphilicity) of PLA2. Therefore, aggregation is a key consequence of the functionally significant interaction of alkyl sulfate monomers along the i-face of PLA2 (Figure 1). The appearance of the aggregate peak shows a steep dependence on the alkyl sulfate concentration (Figures 4 and 6), which implies that either the binding of the amphiphile to the i-face to form $E^{\#}$ or the self-aggregation of $E^{\#}$ is highly cooperative. We are exploring such consequences.

Thr results in Table 1 show that the aggregate size depends on the acyl chain length of the bound alkyl sulfate. In general,

amphiphiles with a cone shape, i.e., polar headgroup larger than the hydrophobic chain, aggregate as micelles. The packing constraints and curvature of such aggregates are also determined by the effective shape of the amphiphile. Comparable geometry is expected to predominate in the aggregates of $E^{\#}$, and differences in the aggregate size are likely to be related to the effective shape of the $E^{\#}$ cone. Shorter alkyl chains form the smaller aggregates with a more curved surface, and vice versa. This is because the ratio of the effective cross-section area of the spatially separated polar to the nonpolar regions of an amphiphile influences the lateral packing constraints that maximize the hydrophobic effect. Comparable factors may be responsible for the PLA2 aggregate sizes of 50−150 kDa reported with a variety of micellar amphiphiles (*18*−*21*, *29*).

It is noteworthy that only a few discrete aggregate sizes are seen with different mutants (Table 2). Also, in the few cases that we have examined (unpublished results) the aggregate size persists above the CMC of the alkyl sulfate. One possible interpretation is that the effective shape of $E^{\#}$, related to the polar to nonpolar cross-sectional area, depends on the number of alkyl sulfates bound along the i-face. A smaller aggregate, favored with a more acute cone angle, would be formed if fewer alkyl sulfates bind to the i-face in $E^{\#}$. Even at this qualitative level of approximation one begins to understand a relationship between the number of alkyl sulfates along the i-face and the size of the aggregate. Since only two or three sizes of aggregates predominate in the perturbed mutants, we suggest that the alkyl sulfate binding along the i-face may occur in two or three steps. The binding may or may not be cooperative in all of these steps. Here the factors that control the aggregate number may be dominated by the ligands for the anion binding to the i-face.

Aggregation of the PLA2 Mutants. Irrespective of the mechanism of the amphiphile interactions along the i-face and self-aggregation of $E^{\#}$, the results in Table 2 clearly show that the aggregate size is influenced by certain critical residues in PLA2. It is intriguing that the substitution of several cationic residues has at best a modest effect on the aggregate size. As pointed out in the preceding section, these results suggest a modest, if any, role for direct electrostatic interactions (*4*). In other words, a loss of the cationic charge on the i-face is probably compensated by other factors associated with the binding of the anionic amphiphiles to the i-face that ultimately leads to aggregation of $E^{\#}$.

Other substitutions that lead to a change in the aggregate size are also indirectly associated with the function of the i-face. Such substitutions are part of an extended hydrogen bond network in IB PLA2 (Figure 7). As suggested originally (*1*, *40*), this network includes a conserved water molecule, NH_2 of A1, ϵNH of H48 via the carboxyl of D99, hydroxyls of Y52 and Y73, and the backbone carbonyls of residues 4, 68, and 71. The network is localized in the domain that is spatially separated from the active site slot. The network is also separated from the anion binding sites along the i-face. This network is to the interior of the protein where the (1,-10)-helix lines the substrate binding slot. Several hydrophobic residues (L2, W3, F5, I9, L19, M20, and F22) make up the i-face and the substrate binding slot that is accessible through the i-face. At least some of these residues make contact with the *sn*-2 acyl chain of the substrate. Despite its suggestive relationship to the active site and i-face, a functional role

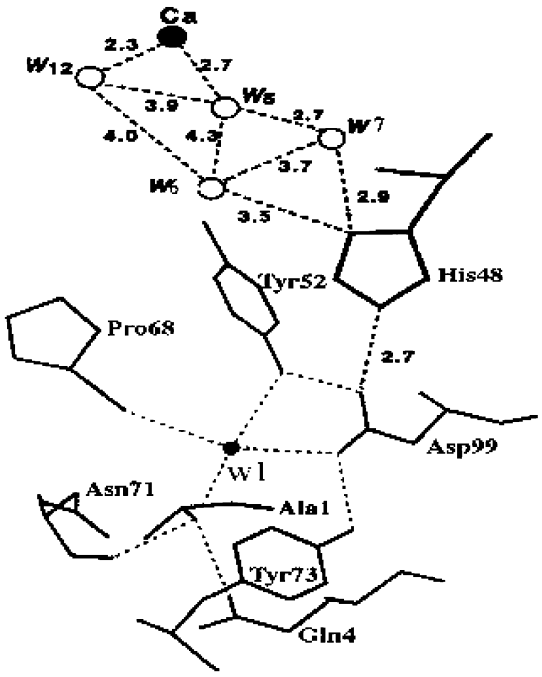

FIGURE 7: Hydrogen-bonding network of pig IB PLA2. Residues (N4, Y52, P68, E71, Y73, D99), a conserved water (W1), and the NH_2 of A1 are H-bonded to a carbonyl oxygen of D99. As a part of the catalytic couple, the other oxygen of D99 is bonded to ϵNH of H48. The δNH of H48 is bonded to the assisting water (W7) bonded to the catalytic water (W5). This figure is based on results in refs *4*, *37*, *45*, and *46*. Note that the positions of W6 and W7 are switched to conform to the earlier assignments (*46*).

for the network of hydrogen bonds has not emerged. A major source of difficulty is that deletion of the individual hydrogen bonds in the network has only a modest effect on the activity measured in some assays and no effect in others (*4*, *28*, *29*, *32*, *36*, *40*−*44*). Such a behavior implies that the role for the participating hydrogen bonds is partially compensated by the interfacial anionic charge.

We propose that the hydrogen bond network controls the affinity and the number of the anionic amphiphiles that interact with the i-face of PLA2. Thus mutations in the residues of the network influence the shape, size, and amphiphilicity (hydrophile−lipophile balance) of $E^{\#}$. Such changes in the effective size and shape of the $E^{\#}$ amphiphile cone would determine the aggregate size. On the basis of this suggestion the kinetic consequences of the perturbed hydrogen bond network would be more apparent under the conditions where the mole fraction or the concentration of the anionic amphiphile is limiting. In fact, the PLA2-catalyzed hydrolysis of zwitterionic substrates is significant only if a sufficient mole fraction of the product fatty acid (or an anionic amphiphile) is present in the interface (*3*, *6*, *16*). Also, the effect of the perturbed hydrogen bond network will not be seen at the tight binding anionic interfaces (*29*, *32*, *36*, *40*−*44*). In fact, this model is also the basis for the choice of the conditions (Figure 6) for screening the perturbed aggregation in the mutants (Table 2).

A Role for the Anion Binding Sites. A role for the anionic charge at the interface in the functional coupling between the events at the i-face and the catalytic site of PLA2 is demonstrated by a variety of observations (*5*, *9*, *11*, *12*). On the basis of the results in Table 2 in general, and the effect of D99A in particular, we propose that perturbations in the

hydrogen bond network around D99 influence the catalytic H48 as well as the ligands for the anion binding at the i-face. Available information suggests that residues around positions 6 and 10 provide ligands for the binding of a cluster of three anions (*37*, *38*, *46*). Such interactions could be influenced by changes in the (1,10)-helix. On one end it is anchored at C11 and on the other to a conserved water (W1 in Figure 7) bound to the NH_2 of A1.

Crystallographic results with the divalent anion-assisted homodimer of PLA2 show that the anions interact mostly through the backbone NH and are not directly charge compensated by the counter charges (*37*, *38*, *46*). A cluster of three of the five coplanar anions in the dimer structure is near the entrance to the substrate binding slot. In pig PLA2 these anions make close contact with the side chain of R6, K10, and also the backbone NH of residues 19 and 20. This is consistent with the suggestion that the binding of pig PLA2 to the anionic interface is mediated through cationic residues in positions 6, 10, and possibly 17 (*29*). Bovine PLA2 with 6N exhibits a comparable aggregation behavior. Therefore, if a net cationic charge is in fact required for the binding of dodecyl sulfate, it is likely to be provided by residues 10 and 17. Irrespective of the fact whether direct electrostatic interaction is needed to fully compensate the anionic charge, the close-range specific interactions of the anionic groups through the backbone and side chain ligands in this region are likely to influence the orientation and position of the N-terminal (1,10)-helix, and vice versa. Substitutions (W3, F5, I9, F22) in this region that influence the aggregate size may also be critical for stabilizing and orienting the water molecules that have close association with the anions. Details of how the hydrogen-bonding network perturbs the amphiphile binding and aggregation remain to be worked out.

Kinetic Consequences of the E# Formation. An outstanding issue of interfacial enzymology is whether an interfacial enzyme can carry out catalytic turnover via a classical monodisperse Michaelis−Menten complex in the aqueous phase. Results with several interfacial enzymes (*3*, *30*, *31*) suggest that the classical solution path for the turnover through the aqueous phase is unlikely. For the reasons uncovered in these studies, virtually all reports of finite monomer rate are suspect. To understand the pro and con arguments, consider the fact that substrates of interfacial enzymes are amphiphiles. If the headgroup of the monodisperse substrate interacts with the i-face, the resulting complex is likely to resemble $E^{\#}$. If so, events of the turnover cycle may not be mediated by the presumed monodisperse enzyme−substrate complex even if virtually all of the excess substrate is monodispersed in the aqueous phase. $E^{\#}$ could stick to the walls of the reaction chamber or adsorb onto the air bubbles (*30*, *31*).

No matter where $E^{\#}$ is localized, the kinetic consequences come from the fact that it could be the only catalytically active form of the enzyme in the reaction mixture. For example, even if the reaction does not occur on the extraneous surfaces, it does not necessarily mean that the turnover occurs through the classical monodisperse Michaelis−Menten complex in the aqueous phase. The behavior of the $E^{\#}$ form of PLA2 with anionic amphiphiles suggests that such an aggregate dispersed in the aqueous phase provides the reaction path for the reported hydrolysis of monodisperse anionic phsopholipids by IB PLA2 (*19*, *20*, *24*) or for the hydrolysis of the zwitterionic substrates by human X PLA2 (*15*). Thus the possibility of formation of $E^{\#}$ under the monomer assay conditions always raises the concern that the Michaelis−Menten complex for the turnover may be in such a complex. Note that at low amphiphile concentrations the $E^{\#}$ complex can exist independently of the aggregate formation. It is quite likely that the amphiphile exchange rate on $E^{\#}$ or its aggregate would be rapid enough to ensure the substrate replenishment to support the turnover rates of several thousands per second (*3*, *5*, *18*, *20*, *24*). It is, however, intriguing to consider the possibility if the turnover characteristics of the Michaelis complex on $E^{\#}$ or on its self-aggregate or on E* are identical.

To recapitulate, approaches aimed at dissecting the interactions along the i-face provide insights into the interactions that lead to the allosteric activation of PLA2. With evidence at hand it is clear that without direct and compelling evidence it cannot be assumed that the reaction catalyzed by an interfacial enzyme in the presence of a monodisperse substrate is necessarily mediated by the monodisperse Michaelis−Menten complex in the aqueous phase. Of course, it is also correct that the formation of $E^{\#}$ with a substrate does not necessarily rule out the possibility for the classical solution path. Direct evidence has to be found in both cases especially if the information is to be used for the study of interfacial activation. Concerns about microstates and microenvironment of the species in the turnover cycle are significant for the kinetic analysis in general and more so for unequivocal identification of the interfacial turnover cycle (*5*). Such concerns also relate to virtually all questions, measures, and criteria used for the analysis of rate activation of an interfacial enzyme.

REFERENCES

1. Verheij, H. M., Slotboom, A. J., and de Haas, G. H. (1981) *Rev. Physiol. Pharmacol. 81*, 91−203.
2. Jain, M. K., Rogers, J. M., Jahagirdar, D. V., Marecek, J. F., and Ramirez, F. (1986) *Biochim. Biophys. Acta 860*, 435−447.
3. Jain, M. K., and Berg, O. G. (1989) *Biochim. Biophys. Acta 1002*, 127−156.
4. Berg, O. G., Tsai, M.-D., Gelb, M. H., and Jain, M. K. (2001) *Chem. Rev. 101*, 2613−2653.
5. Berg, O. G., and Jain, M. K. (2001) *Interfacial Enzyme Kinetics*, pp 302, John Wiley & Sons, London.
6. Jain, M. K., Egmond, M. R., Verheij, H. M., Apitz-Castro, R. J., Dijkman, R., and de Haas, G. H. (1982) *Biochim. Biophys. Acta 688*, 341−348.
7. Jain, M. K., Ranadive, G. N., Rogers, J. M., Yu, B. Z., and Berg, O. G. (1991) *Biochemistry 30*, 7306−7317.
8. Yu, B. Z., Berg, O. G., and Jain, M. K. (1993) *Biochemistry 32*, 6485−6492.
9. Berg, O. G., Rogers, J. M., Yu, B. Z., Yao, J., Romsted, L. S., and Jain, M. K. (1997) *Biochemistry 36*, 14512−14530.
10. Rogers, J. M., Yu, B. Z., Tsai, M.-D., Berg, O. G., and Jain, M. K. (1998) *Biochemistry 37*, 9549−9556.
11. Yu, B. Z., Poi, M. J., Ramagopal, U. A., Jain, R., Ramakumar, S., Berg, O. G., Tsai, M.-D., Sekar, K., and Jain, M. K. (2000) *Biochemistry 39*, 12312−12323.
12. Ramirez, F., and Jain, M. K. (1991) *Proteins 9*, 229−239.
13. Valentin, E., and Lambeau, G. (2000) *Biochim. Biophys. Acta 1488*, 59−70.
14. Bezzine, S., Koduri, R. S., Valentine, E., Murakami, M., Kudo, I., Ghomoshch, F., Sadilek, F., Lambeau, G., and Gelb, M. H. (2002) *J. Biol. Chem. 275*, 3179−3191.
15. Pan, Y. H., Yu, B.-Z., Singer, A. G., Ghomashchi, F., Lambeau, G., Gelb, M. H., Jain, M. K., and Bahnson, B. J. (2002) *J. Biol. Chem. 277*, 20986−20993.
16. Apitz-Castro, R. J., Jain, M. K., and de Haas, G. H. (1982) *Biochim. Biophys. Acta 688*, 349−356.

17. Bayburt, T., Yu, B. Z., Lin, H., Browning, J., Jain, M. K., and Gelb, M. H. (1993) *Biochemistry 32*, 573−582.
18. Hille, J. D. R., Donne-Op den Kelder, G., Sauve, M., de Haas, G. H., and Egmond, M. R. (1981) *Biochemistry 20*, 4068−4073.
19. Van Oort, M. G., Dijkman, R., Hille, J. D. R., and de Haas, G. H. (1985) *Biochemistry 24*, 7987−7993.
20. Van Oort, M. G., Dijkman, R., Hille, J. D. R., and de Haas, G. H. (1985) *Biochemistry 24*, 7993−7999.
21. Deveer, A. M. Th. J., Dijkman, R., Leuveling-Tjeenk, M., Van der Berg, L., Ransac, S., Batenberg, M., Egmond, M., Verheij, H., and de Haas, G. H. (1991) *Biochemistry 30*, 10034−10040.
22. Van Eijk, J. H., Verheij, H. M., Dijkman, R., and de Haas, G. H. (1983) *Eur. J. Biochem. 132*, 183−190.
23. Van Eijk, J. H., Verheij, H. M., and de Haas, G. H. (1984) *Eur. J. Biochem. 140*, 407−413.
24. Rogers, J., Yu, B.-Z., and Jain, M. K. (1992) *Biochemistry 31*, 6056−6062.
25. Yuan, W., Quinn, D. M., Sigler, P. B., and Gelb, M. H. (1990) *Biochemistry 29*, 6082−6088.
26. Lefkowitz, L. J., Deems, R. A., and Dennis, E. A. (1999) *Biochemistry 38*, 14174.
27. Kilby, P. M., Primrose, W. U., and Roberts, G. C. K. (1995) *Biochem. J. 305*, 935−942.
28. Janssen, M. J. W., Burghout, P. J., Verheij, H. M., Slotboom, A. J., and Egmond, M. R. (1999) *Eur. J. Biochem. 263*, 782−790.
29. de Haas, G. H., Van Scharrenburg, G. J. M., and Slotboom, A. J. (1987) *Biochemisty 26*, 3402−3406.
30. Berg, O. G., Cajal, Y., Butterfoss, G. L., Grey, R. L., Alsina, M. A., Yu, B. Z., and Jain, M. K. (1998) *Biochemistry 37*, 6615−6627.
31. Yu, B. Z., Berg, O. G., and Jain, M. K. (1999) *Biochemistry 38*, 10449−10456.
32. Yu, B. Z., Rogers, J. M., Tsai, M.-D., Pidgeon, C., and Jain, M. K. (1999) *Biochemistry 38*, 4875−4884.
33. Jain, M. K., and Vaz, V. L. C. (1987) *Biochim. Biophys. Acta 905*, 1−8.
34. Jain, M. K., Rogers, J. M., and de Haas, G. H. (1988) *Biochim. Biophys. Acta 940*, 51−62.
35. Yu, B. Z., Berg, O. G., and Jain, M. K. (1993) *Biochemistry 32*, 6485−6492.
36. Jain, M. K, and Maliwal, B. P. (1993) *Biochemistry 32*, 11838−11846.
37. Pan, Y. H., Epstein, T. M., Jain, M. K., and Bahnson, B. J. (2001) *Biochemistry 40*, 609−617.
38. Epstein, T. M., Yu, B.-Z., Pan, Y. H., Tutton, S. P., Maliwal, B. P., Jain, M. K., and Bahnson, B. J. (2001) *Biochemistry 40*, 11411−11422.
39. Homan, R., and Jain, M. K. (2000) in *Intestinal Lipid Metabolism* (Mansbach, C. M., Tso, P., and Kuksis, A., Eds.) pp 81−104, Kluwer Academic Press and Plenum Publications, New York.
40. Verheij, H. M. (1995) in *Phospholipase A2 in Clinical Inflammation: Molecular Approaches to Pathophysiology* (Glaser, K. B., and Vadas, P., Eds.) pp 3−24.
41. Dupureur, C. M., Yu, B. Z., Jain, M. K., Noel, J. P., Deng, T., Li, Y., Byeon, I. T., and Tsai, M.-D. (1992) *Biochemistry 31*, 6402−6413.
42. Maliwal B. P., Yu, B. Z., Szacinski, H., Squier, T., van Binsbergen, J., Slotboom, A. J., and Jain, M. K. (1994) *Biochemistry 33*, 4509−4516.
43. Liu, X., Zhu, H., Huang, B., Rogers, J. M., Yu, B. Z., Kumar, A., Jain, M. K., Sundaralingam, M., and Tsai, M.-D. (1995) *Biochemistry 34*, 7322−7334.
44. Jain, M. K., Maliwal, B. P., de Haas, G. H., and Slotboom, A. J. (1986) *Biochim. Biophys Acta 860*, 448−461.
45. Yu, B. Z., Rogers, J., Nicol, G., Theopold, K. H., Seshadri, K., Vishweshwara, S., and Jain, M. K. (1998) *Biochemistry 37*, 12576−12587.
46. Pan, Y. H., Yu, B. Z., Beg, O. G., Jain, M. K., and Bahnson, B. J. (2002) *Biochemistry 41*, 14790−8000.

BI034232X